

Weyl Semimetallic Phase in High Pressure CrSb₂ and Structural Compression Studies of its High Pressure Polymorphs

Carl Jonas Linnemann^a, Emma Ehrenreich-Petersen^{a,b}, Davide Ceresoli^c, Timofey Fedotenko^b, Innokenty Kantor^d, Mads Ry Vogel Jørgensen^{a,d}, Martin Bremholm^{a,*}

^a*Department of Chemistry and iNANO, Aarhus University, Langelandsgade 140, 8000, Aarhus C, Denmark*

^b*Deutsches Elektronen-Synchrotron DESY, Notkestr. 85, 22607, Hamburg, Germany*

^c*Consiglio Nazionale delle Ricerche - Istituto di Scienze e Tecnologie Chimiche "G. Natta", via Golgi 19, 20133, Milano, Italy*

^d*MAX IV Laboratory, Lund University, Fotongatan 2, Lund, 225 94, Sweden*

Abstract

In this study, high pressure synchrotron powder X-ray diffraction is used to investigate the compression of two high pressure polymorphs of CrSb₂. The first is the CuAl₂-type polymorph with an eight-fold coordinated Cr, which can be quenched to ambient conditions from high-pressure high-temperature conditions. The second is the recently discovered MoP₂-type polymorph, which is induced by compression at room temperature, with a seven-fold coordinated Cr. Here, the assigned structure is unambiguously confirmed by solving it from single-crystal X-ray diffraction. Furthermore, the electrical properties of the MoP₂-type polymorph were investigated theoretically and the resistance calculations under pressure were accompanied by resistance measurements under high pressure on a single crystal of CrSb₂. The calculated electronic band structure for the MoP₂-type phase is discussed and we show that the polymorph is semimetallic and possesses type-I Weyl points. No further phase transitions were observed for the CuAl₂-type structure up to 50 GPa and 40 GPa for the MoP₂-type structure. Even though the CuAl₂-phase has the highest coordination number of Cr, it was found to be less compressible than the MoP₂-phase having a seven-fold coordinated Cr, which was attributed to the longer Cr-Sb distance in the CuAl₂-type phase. The discovery of a type-I Weyl semimetallic phase redin CrSb₂ opens up for discovering other Weyl semimetals in the transition metal di-pnictides under high pressure.

Keywords: Crystal binding and equation of state, Electronic band structure, Phase transitions, High pressure, X-ray diffraction

*Corresponding author

Email address: bremholm@chem.au.dk (Martin Bremholm)

1. Introduction

Many redcompounds exist in different polymorphs with different properties, such as WP_2 , which exists in the low temperature modification α - WP_2 [1] and the high temperature modification β - WP_2 crystallizing in the $Cmc2_1$ space group [2]. Both polymorphs are semimetals where β - WP_2 is a type-II Weyl semimetal and α - WP_2 is a trivial semimetal [3, 4]. Pressure can also induce phase transitions such as in $CrSb_2$ where, recently, a new high pressure polymorph was discovered independently by Li et al. as well as Ehrenreich-Petersen et al., extending the number of known polymorphs of $CrSb_2$ to three [5, 6]. At ambient pressure $CrSb_2$ crystallizes in the marcasite structure (Fig. 1 a)) and has an antiferromagnetic (AFM) ordering below $T_N \approx 273$ K, with a $1 \times 2 \times 2$ supercell with the magnetic moments perpendicular to the (101) plane [7]. The marcasite phase is a n -type semiconductor with a narrow bandgap of 0.1 eV redand has been shown to possess large anisotropic magnetoresistance in its surface states [8, 9]. The first high-pressure polymorph of $CrSb_2$ (herein named HP-I) was discovered by Takizawa et al. by high pressure synthesis above 5.5 GPa and 600 °C [10]. This polymorph crystallizes in a $CuAl_2$ -type structure (Fig. 1 b)), redin which $TiSb_2$ and Vsb_2 also crystallize [11]. Here, $TiSb_2$ has been shown to be a three-dimensional Dirac-semimetal [12]. redThe HP-I phase of $CrSb_2$ exhibits metallic behaviour and is an itinerant electron ferromagnet with a Curie temperature of approximately 160 K [13]. At approximately 90 K it has an AFM spin density wave transition, which can be suppressed under the application of magnetic fields. It has been shown that at pressures above 0.5 GPa the two states merge together to a single AFM state, where the AFM order is suppressed to lower temperatures by application of pressure and vanishes completely at $P_c \approx 9$ GPa, indicating an AFM quantum critical point [14]. The newly discovered high pressure polymorph (herein named HP-II) has been shown to appear at room temperature and pressures above 10 GPa. It is meta-stable and cannot be recovered to ambient pressure [5, 6]. Furthermore laser-heating experiments under high pressure have shown that the phase transforms into the high-pressure $CuAl_2$ -type phase, indicating a high activation barrier for the phase transition to the HP-I phase and that it is more stable than the HP-II phase [6]. Li et al. showed that the polymorph exhibits n - p conduction switching as well as that the high pressure phase exhibits metallic conduction [5]. There have been disagreements regarding the structure, where Li et al. assigned it to the arsenopyrite structure-type, while Ehrenreich-Petersen et al. assigned it to have a MoP_2 -type structure using a combination of DFT calculations and powder diffraction [5, 6]. The MoP_2 -type structure has the orthorhombic $Cmc2_1$ space-group, where Mo is coordinated to seven P atoms. This structure is furthermore isostructural with β - WP_2 , and both MoP_2 and β - WP_2 have been studied immensely as they are robust type-II Weyl-semimetals [2, 3]. Both materials have been shown to possess extremely high magnetoresistance and high conductivity[15]. redFurthermore, high harmonic generation up to the 10th order

has been shown for β -WP₂ [16] and due to their high magnetoresistance both materials are potential candidates for high-gain high-frequency amplifiers with low power dissipation, which could replace High-electron-mobility transistors in quantum computers [17]. For both compounds no structural phase transitions under the application of pressure have been shown, however β -WP₂ has been shown to possess a pressure induced Lifshitz transition [18, 19]. Both MoP₂ and WP₂ have also shown to crystallize in the monoclinic OsGe₂-type structure. For WP₂ it is a low temperature modification, while it for MoP₂ has been shown to be a recoverable high-pressure high-temperature polymorph [2, 18].

In this study the high pressure structural properties of both high pressure polymorphs of CrSb₂ are investigated experimentally through powder diffraction at high pressures as well as theoretically through density functional theory (DFT) calculations. Furthermore, the MoP₂-type structure is shown to be the correct structure for the HP-II polymorph of CrSb₂ through single crystal X-ray diffraction at 12 GPa. The electronic properties of this polymorph are furthermore investigated through resistance measurements under high pressure at ambient temperature accompanied by theoretical calculations regarding the resistivity and Hall coefficients. The band structure is calculated at 12 GPa and the topology of the band crossings is determined to examine if the HP-II phase possesses Weyl points. The verification of the MoP₂-type structure, and furthermore the evidence of Weyl-points opens up for discovering other high pressure transition-metal di-pnictides, which potentially host Weyl points.

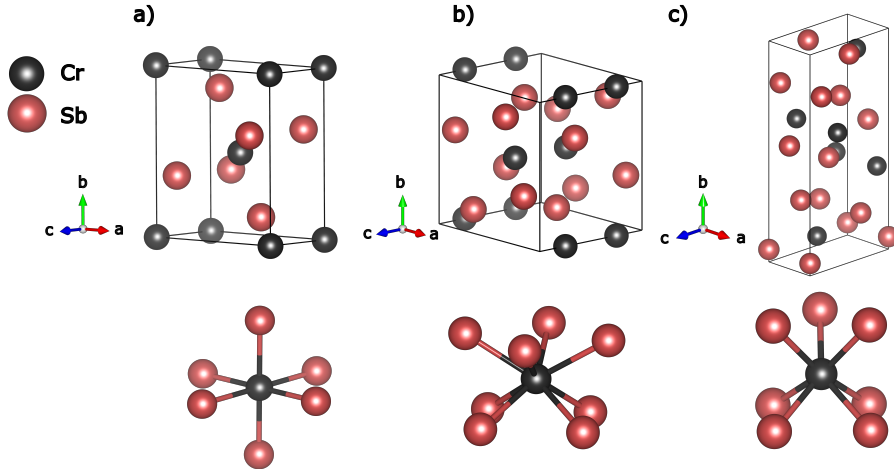


Figure 1: Crystal structure and Cr coordination of the different high-pressure polymorphs of CrSb₂: **a)** Marcasite, **b)** CuAl₂-type (HP-I) and **c)** MoP₂-type (HP-II).

2. Materials and methods

2.1. Powder synthesis of CrSb_2

Stoichiometric amounts of Cr (99.95%) and Sb (99.95%) were ground in a mortar, pressed to a pellet and sealed in an evacuated quartz tube, which was heated at a rate of 50 °C/min to 600 °C, kept at that temperature for 48 h and then quenched in air.

2.2. Single crystal growth of CrSb_2

Single crystals of CrSb_2 were grown using a flux method adapted from Ref. [8]. Cr (99.95%) and Sb (99.99%) with a molar ratio of 6:94 were ground in a mortar and sealed in an evacuated quartz tube. The tube was heated to 1000 °C at 50 °C/min, kept at that temperature for 36 h followed by cooling to 640 °C at 2 °C/h and then cooled to room temperature. The crystals were isolated from the Sb-flux through centrifugation. The phase purity of the crystals was verified by determining the unit cell of a single crystal using a STOE Stadivari single crystal diffractometer with Mo K- α radiation (Table S1).

2.3. High pressure synthesis of CuAl_2 -type CrSb_2

A pellet of marcasite CrSb_2 powder was loaded in a large volume press in a 14/8 COMPRES octahedral assembly [20], pressurized to 7 GPa at 1 GPa/h and heated to 900 °C for 1 h followed by quenching. The phase purity of the sample was verified using powder X-ray diffraction using a Rigaku Smartlab diffractometer with Co K- $\alpha_{1,2}$ radiation (Fig. S1).

2.4. High pressure diffraction measurements

Single-crystal X-ray diffraction (SC-XRD) measurements under high pressure were conducted at the Extreme Conditions Beamline (ECB, P02.2)[21], PETRA III, DESY ($\lambda=0.2899$ Å, beam size $\approx 2 \times 2.7$ μm^2 , Perkin Elmer XRD 1621 detector). Three single crystals of CrSb_2 were loaded in a plate-diamond anvil cell (DAC) (Almax EasyLab) with 600 μm culet diamonds. Additionally, a small ruby sphere was loaded that served as the pressure calibrant during the experiment by the ruby fluorescence method [22]. A 16:3:1 mixture of methanol-ethanol-water was used as the pressure transmitting medium (PTM). A stainless-steel gasket pre-indented to 72 μm micron with a 300 μm hole drilled by electric discharge machining (EDM), served as the sample chamber. The pressure was increased to 12 GPa, i.e. above the structural phase transition of CrSb_2 and the DAC was heated to 100 °C for one hour to relieve strain. The pressure was allowed to equilibrate for several hours before the measurement and was measured right before and after the diffraction experiment with no observed pressure deviation. As most of the single crystals had split into separate crystal domains during the phase transition a suitable spot for diffraction was chosen and diffractograms were obtained with a rotation from -37° to 37° with 0.5° steps with an acquisition time of 0.5 s and a 50 μm Pt absorber inserted in the beam. Reduction and integration of the data was performed using CrysAlisPro [23] and the structure

was solved using SHELXT in Olex2 and refined using SHELXL [24, 25, 26]. During integration and reduction of the data, frames with a R_{int} above 0.3 were rejected.

Membrane driven Mao-Bell type DACs with culet sizes of 300 μm (For the HP-I phase) or 200 μm (For the HP-II phase) were used for the high pressure powder X-ray diffraction measurements (HP-PXRD). Re gaskets indented from approx. 250 μm to approx. 40 μm were used with a 120 μm hole drilled by EDM for the HP-I phase and a laser-drilled 100 μm hole for the HP-II phase. Silicone oil was used as the PTM for the HP-I phase and for the HP-II phase Ne was gas-loaded as the PTM using the gas-loading system at Sector 13, APS [27]. To obtain small grain sizes, the samples were suspended in ethanol and the supernatant was removed and dried. Thin sheets of samples were loaded together with thin sheets of Cu (for the HP-I phase) or Au (for the HP-II phase) for pressure determination [28, 29]. A small ruby sphere was also added, which served to determine the pressure during the loading and closing of the cell. For the HP-I phase the HP-PXRD measurements were conducted at the DanMAX beamline at the MAX IV synchrotron ($\lambda=0.3542$ Å, beam size $\approx 7.4 \times 7.2$ μm^2 , Dectris Pilatus3X 2M CdTe detector). The diffractograms for the HP-II phase have been shown, but not refined, in Ref. [6], and the HP-PXRD measurements for the HP-II phase of CrSb_2 were conducted at the Advanced Photon Source at the GSECARS beamline 13-ID-D ($\lambda=0.3344$ Å, beam size $\approx 4 \times 3$ μm^2 , Dectris Pilatus CdTe 1M detector). All 2D powder diffractograms were integrated using Dioptas [30]. Le Bail refinements of the unit cell parameters were performed using the FullProf suite [31] and the unit cell parameters were fitted to the third order Birch-Murnaghan equation of state (EoS) using the EoSFit7 GUI [32]. Crystal structure models were drawn using the VESTA software [33].

2.5. Resistance measurement of CrSb_2 under pressure

The resistance measurements were performed using an iDiamond (Almax EasyLab) containing eight tungsten microprobes partially embedded in an epitaxially grown diamond [34]. The culet size of the anvil was 250 μm with bevels. A BX-90 DAC was used with a stainless-steel gasket indented from 250 μm to 50 μm using two standard diamond anvils redin order not to damage the electrodes on the iDiamond. A hole with a diameter of 120 μm was drilled using EDM. Steatite was used as the pressure transmitting medium. A suitable single crystal of CrSb_2 was mounted on the designer anvil together with a ruby for pressure determination [22] and the resistance was measured in a two-wire reedirect-current geometry with a current of 1 mA using a Keithley 2450 sourcemeter.

2.6. DFT modeling

DFT calculations were performed with the plane wave pseudopotential code Quantum Espresso [35, 36] with ultrasoft pseudopotentials and the PBEsol exchange-correlation functional [37]. The plane wave and density cutoffs were 45 and 450 Ry, respectively. In all calculations we sampled the reciprocal space with a nearly constant density of k-points of $\simeq 0.2$ Å⁻¹. We used a Gaussian smearing

of 0.005 Ry for the electronic temperature. Within our DFT setup, the band gap of the AMFe marcasite structure is 0.06 eV, which slightly underestimates the experimental value of 0.07 eV [38]. A Hubbard U correction of 2.3 eV as in Ref. [38] results in a worse agreement with the experimental AFMe lattice parameters, and, contrary to Ref. [38], the AFMe marcasite structure becomes metallic, with Sb-5*p* orbital bands crossing the Fermi level. As a function of pressure, variable-cell geometry optimizations of CrSb₂ were performed in three magnetic ground states: non-magnetic (NM), ferromagnetic (FM), and antiferromagnetic (AFM). For the marcasite structure we used the AFMe ordering reported in Ref. [38]. For the HP-II structure we generated all AFM orderings compatible with a 2×2×2 supercell and selected the lowest energy one (which we named AFM1, Fig. S2).

The electrical conductivity was calculated with the BoltzTraP2 code [39] at 300 K in the Constant Relaxation Time Approximation (CRTA), with a 20×20×20 k-point mesh. The search for Weyl points requires the evaluation of the DFT Hamiltonian on an extremely dense k-point grid. For this purpose, we used PAOFLOW2 [40] to construct a tight-binding Hamiltonian from the self-consistent plane wave Hamiltonian. The BFGS algorithm is used to locate band crossings in reciprocal space. Finally, the chirality (i.e. the \mathbb{Z}_2 invariant) of each band crossing was calculated using Z2PACK [41].

3. Results and discussion

3.1. The crystal structure of the HP-II phase obtained from single-crystal X-ray diffraction

The results from the SC-XRD refinement are shown in Table 1 together with the results from the DFT-calculations and powder diffraction from Ehrenreich-Petersen et al. [6]. Here, the structural solution from the single crystals of CrSb₂ at 12 GPa shows that the HP-II structure is of the MoP₂-type in agreement with our previous paper [6].

3.2. Electrical properties of the HP-II phase

The electrical resistance of the HP-II phase was measured for pressures up to 21 GPa and is shown in Fig. 2a) together with the calculated resistivity. Between 5 and 10 GPa a small linear decrease of the resistance is observed, which was also observed by Li et al. indicating a decrease of the band-gap of the marcasite phase with pressure, which also has been shown for some pressure intervals in FeSb₂ [42, 43]. After the onset of the phase transition at 10 GPa [6], a sharp decrease of the resistance is observed, indicating a metallization of the system. The residual resistance of 130 Ω after the phase transition is high for a metal, which is attributed to the resistance in the electrodes, which for a similar anvil has been reported to be 110 Ω [34].

The evolution of the electronic density of states as a function of pressure is shown in Fig. S3 for the marcasite- and the HP-II polymorph. As reported in Ref. [38], in the marcasite structure the magnetic order has a very strong impact

Table 1: Results from the single-crystal diffraction experiment compared to the data from DFT and powder diffraction from ref. [6]

	Single crystal diffraction	Ref. [6] ^a
Pressure (GPa)	11.9(2)	12.0(7)
Space group	<i>Cmc2₁</i>	<i>Cmc2₁</i>
<i>a</i> (Å)	3.0752(2)	3.06723(6)
<i>b</i> (Å)	12.4476(19)	12.4495(5)
<i>c</i> (Å)	5.8741(2)	5.85682(9)
α, β, γ (°)	90	90
<i>V</i> (Å ³)	224.85(4)	223.645(11)
<u>Atomic coordinates</u>		
Cr	(0, 0.3942(5), 0.1490(6))	(0, 0.39431, 0.15191)
Sb1	(0, 0.20702(17), 0.3545(2))	(0, 0.20806, 0.36102)
Sb2	(0, 0.05627(18), 0)	(0, 0.05501, 0)
<u>Refinement statistics</u>		
Completeness	55.9%	
<i>I</i> / σ (<i>I</i>)	95.7	
<i>R</i> ₁ (%)	5.82	
<i>wR</i> ₂ (%)	16.10	
<i>R</i> _{int} (%)	0.62	
Goof	1.150	
λ (Å)	0.2899	

^a The unit cell was standardized to match the setting from the single-crystal diffraction experiment.

on the electronic structure and the experimental AFMe order opens a ~ 0.2 eV gap between the Cr-projected valence and conduction states. GGA calculations (as in the present case) predict a vanishing band gap, with a low density of states and low electron velocity. On the contrary GGA+U calculations [38] produce a narrow band of 0.35 eV, which overestimates the experimental band gap of ~ 0.07 eV. Upon increasing pressure, the density of states reveals that a pseudogap is generated by the splitting of 3*d* Cr orbitals. In the marcasite structure, the band edges near the Fermi level have a large Cr-3*d* character, while the Sb atomic orbitals contribute largely to the electronic properties below -2 eV and above $+3$ eV from the Fermi level (not shown in the figure). Overall, this results in a semi-metallic or semi-conducting behaviour. The situation is strikingly different for the HP-II polymorph. First, the system is metallic with a large density of states at the Fermi level, and the magnetic order has a modest impact on the electronic structure. The density of states of the HP-II structure at E_F decreases as a function of pressure. The results thus confirm that the marcasite to HP-II transition is accompanied by a sudden metallization of the system. This leads to the lower resistivity of the HP-II phase compared to the marcasite phase. Furthermore, the drop of the resistance between 5 and 10

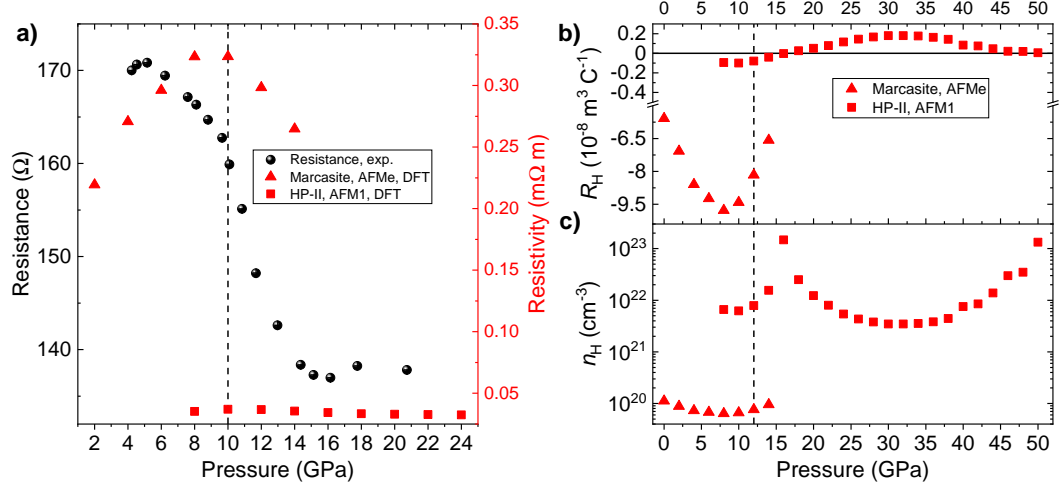


Figure 2: a) Resistance of CrSb₂ under high pressure: The experimentally measured resistance of CrSb₂ under the phase transition to the MoP₂-structure is shown together with the calculated resistivity for the marcasite phase and the MoP₂-type phase. The dashed line marks the onset of the phase transition from the marcasite to the HP-II phase [6]. b) Calculated Hall coefficient. The dashed line marks the phase transition pressure from DFT [6] and the line at $R_H = 0$ serves as a guide to the eye. c) The carrier concentration calculated from the Hall coefficient.

GPa for the marcasite phase is also reproduced by the calculations, however with a pressure offset of 4 GPa. The calculated Hall-coefficient (Fig. 2 b)) is in accordance with the measurements by Li et al. [5] with a change to a positive Hall coefficient after the phase transition. The carrier concentration obtained from the Hall coefficient (Fig. 2 c)) is on the same order of magnitude as in Li et al., however our calculated maximum is 4 GPa lower than the observed maximum by Li et al.[5] which is attributed to computational effects as well as effects of non-hydrostaticity in the measurements. The fact that the calculations on the MoP₂-type model for the high-pressure phase are consistent with the results by Li et al. provides further evidence that the MoP₂-type structure is correct. The band structure of the AFM1 structure at 12 GPa is shown in Fig. 3 both with and without Spin Orbit Coupling (SOC). The effect of SOC is minor in this system and it results in narrow splittings of the bands in the vicinity of the Fermi level. At 12 GPa the system is a semimetal with a pseudogap and low density of states at the Fermi level (Fig. S3). The AFM1 magnetic order removes the C centering from the $Cmc2_1$ space group. Even though the space group is non-symmorphic, we verified that the system is not an *altermagnet* [44, 45], i.e. that no spin-splitting occurs at any k-point of the Brillouin zone. The large number of band crossings or near-crossings around the Fermi level, could reveal the presence of Weyl points. Similarly to the parent structure compounds, MoP₂ and WP₂ [3], we found two symmetry independent type-I Weyl points. The results are reported in Table 2. From Fig. 4 a) w_1 points are located near to the top and bottom face of the Brillouin zone. Due to the orthorhombic symmetry,

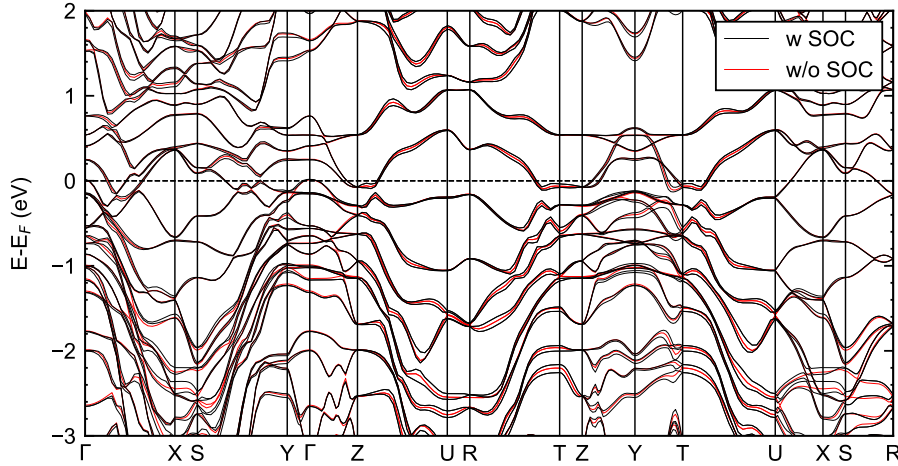


Figure 3: Band structure of the HP-II AFM1 structure at 12 GPa around the Fermi level, with and without Spin Orbit Coupling (SOC).

w_1 points with opposite chirality sit aligned along the b_2 and b_3 reciprocal lattice vectors. The w_2 points are instead located near the $k_z = 0$ ($b_3 = 0$) plane and are composed by very close pairs, as in MoP₂. As the w_2 points have the same chirality they are robust with respect to strain and small deformations. The band structure passing through the w_1 and w_2 points reveals tilted cones (Fig. 4 b-c)), with just one point crossing the constant energy plane (type-I Weyl points).

Table 2: Coordinates, chirality and energy of Weyl points in the HP-II AFM1 structure at 12 GPa. For each point listed, the remaining 7 ones are generated by applying the mirror symmetries.

Weyl point	k_x (\AA^{-1})	k_y (\AA^{-1})	k_z (\AA^{-1})	Chirality	$E-E_F$ (eV)
w_1	0.2141	0.0792	0.4625	+1	-0.1271
w_2	0.3729	0.1096	0.0055	+1	-0.1129

3.3. Equation of state of the high pressure polymorphs of CrSb₂

The diffractograms for the HP-II structure are shown in Fig. 5 a) and the refined unit cell parameters are shown together with the values from the DFT calculations in Fig. 5 b-e) together with the Birch-Murnaghan EoS fits (Table 3 for the volume and redTable S3 in the SI for the linear moduli). The volume decreased with pressure in a scattered way, which is attributed to strain observed for the Au pressure standard as well as a change in the measured sample position at 19.3 GPa and change in the measured Au position at 21.7 GPa. From the linear moduli the b -axis was seen to be the least compressible

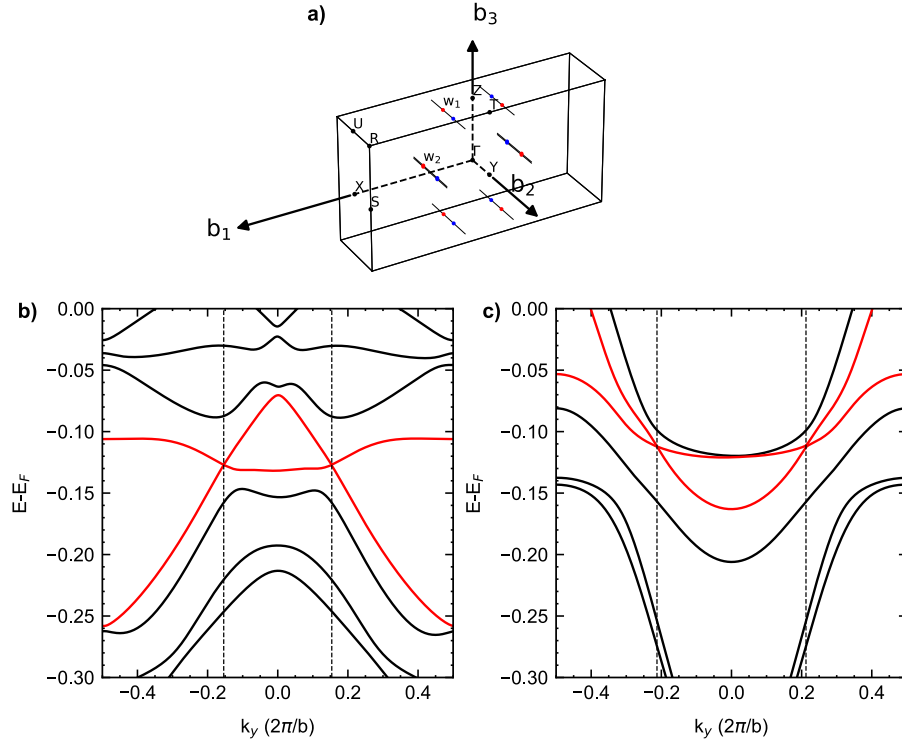


Figure 4: a) Brillouin zone of the HP-II AFM1 structure at 12 GPa with Weyl points w_1 and w_2 . Red points have positive chirality, blue points have negative chirality. The w_2 points are very close to the $b_3=0$ ($k_z=0$) plane. b) Band structure passing through the w_2 points. c) Band structure passing through the w_1 points.

while the c -axis was the most compressible. As the angle between the bond of the Sb-Sb dimer and the b -axis and c -axis is approx. 45° , this bond stabilizes both axes equally. Therefore, the lower compressibility of the b -axis is attributed to the compression of the Cr-Sb bonds, as they are oriented more along the b - than the c -axis. Along the a -axis both the Cr-Cr and Sb-Sb bond distances are equal to the lattice constant, and here the intermediate compressibility is attributed to the Cr-Cr interactions. The parent compounds, MoP₂ and redWP₂, have a higher bulk modulus, redhowever the same trend for the linear moduli with $M_{0,b} > M_{0,a} > M_{0,c}$ is also seen for MoP₂ redand WP₂ [19, 46].

For the HP-I structure the diffractograms are shown in Fig. 6 a). The refined unit cell parameters and the unit cell parameters calculated by DFT are shown in Fig. 6c) together with the Birch-Murnaghan EoS fits (Table 3 for the volume and redTable S4 in the SI for the linear moduli). The a - and c -axis were seen to decrease relatively smoothly with pressure, while for the volume some points around 5-15 GPa were scattered around the fit. The obtained ambient

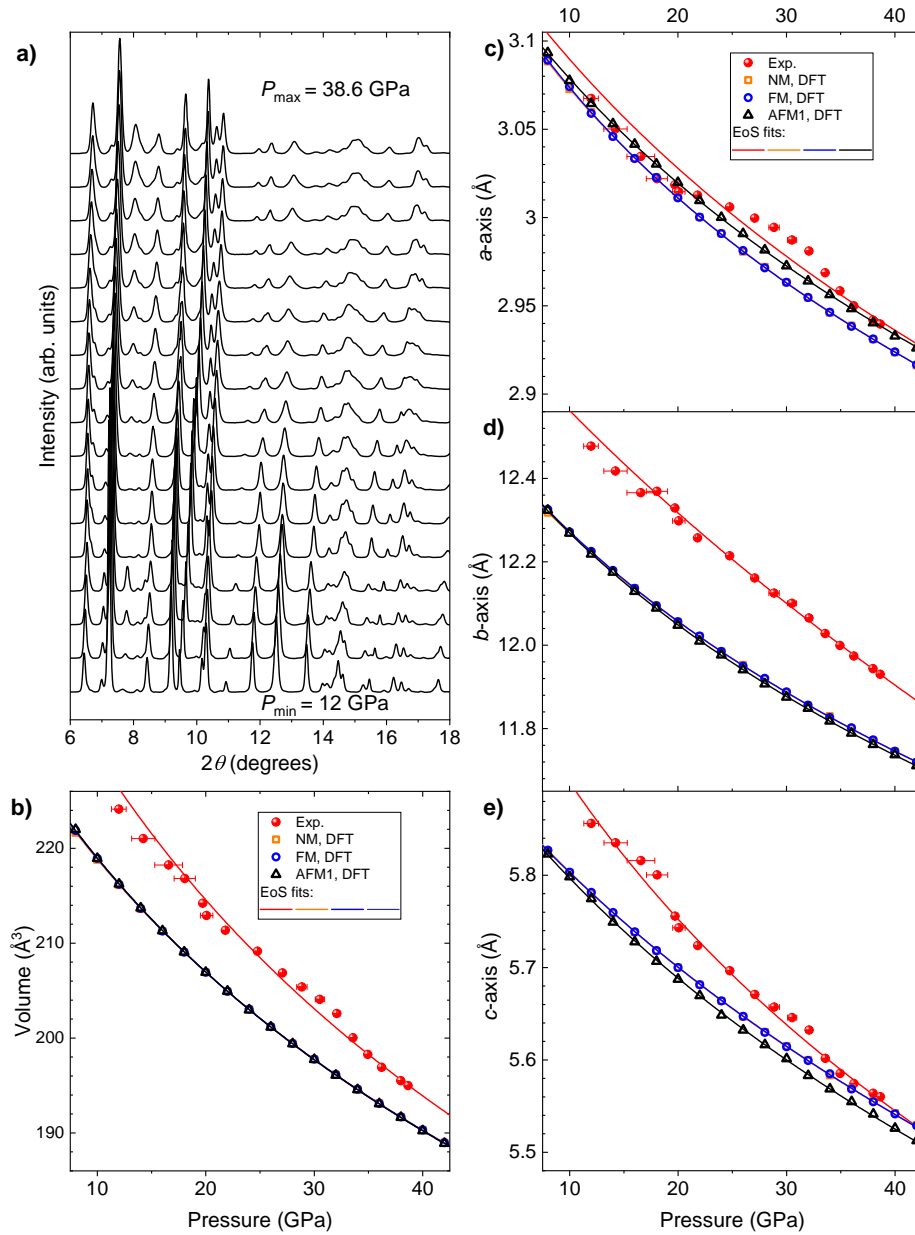


Figure 5: a) Background subtracted waterfall plot of the diffractograms for the HP-II phase. b-e) Experimental and calculated unit cell parameters for the HP-II structure.

pressure unit cell values (Table S4 and Table 3 for the volume) are in good agreement with the values obtained by Takizawa et al. and Jiao et al. [10, 13, 14].

From the obtained linear moduli the c -axis was seen to be more compressible

Table 3: Equation of state parameters for both high pressure polymorphs of CrSb₂ as well as for related structures.

	V_0 (Å ³)	K_0 (GPa)	K'_0	Comments
<u>CuAl₂-type structures:</u>				
HP-I CrSb ₂	241.68(15)	77(2)	6.2(3)	This study
TiSb ₂		91 ^a		Tavassoli et al. [47]
V _{0.97} Sb ₂		85 ^a		Failamani et al. [48]
CuAl ₂	179.5(6)	117(13)	4 (fixed)	Grin et al. [49]
<u>MoP₂-type structures:</u>				
HP-II CrSb ₂	251.8(14)	91(3)	4 (fixed)	This study
MoP ₂		238(20)		Soto et al. [46]
redWP ₂	red174.8(2)	red234.0(34)	red4(fixed)	redChi et al. [19]
<u>Marcasite-type:</u>				
CrSb ₂	137.2(2)	33(3)	13.6(19)	Ehrenreich-Petersen et al. [6]
	130.7(2)	74.2(2)	4 (fixed)	Li et al. [5]

^a Measured by resonant ultrasound spectroscopy

red than the a -axis, which also has been reported for TiSb₂ by Armbrüster et al. which they attributed to weaker Ti-Ti bonds compared to the Sb-Sb bonds [11]. By comparing the HP-I phase to its isostructural compounds TiSb₂ and V_{1-x}Sb₂ a decreasing trend in bulk modulus (Table 3) is seen going from Ti-V-Cr. As the bulk modulus of the elements increases from Ti-V-Cr [50, 51, 52], and the M -Sb distance (M =Ti, V, Cr) decreases when going from Ti-V-Cr an increasing trend in the bulk modulus would be expected. However, the Sb-Sb distance decreases when going in this direction, and as the Sb-Sb bond had been shown to be the least compressible, this increase in bond distance explains the decreasing bulk modulus and furthermore verifies that the Sb-Sb bond is the least compressible [10, 11].

3.4. Discussion of bulk moduli among the polymorphs of CrSb₂

In Table 4 selected bond distances for the three polymorphs are shown. To facilitate a better comparison among the polymorphs, the atomic coordinates from the SC-XRD experiment were used for the unit cell extrapolated to 0 GPa for the HP-II phase. At 0 GPa the Cr-Sb distance in the HP-II polymorph is similar to the Cr-Sb distance in the marcasite phase, where the coordination number is six. Thereby the higher bulk-modulus of the HP-II phase can be explained by its higher coordination number of seven. In the HP-I phase Cr is coordinated to eight Sb atoms, however the bulk modulus for this polymorph is lower than for the HP-II phase, which is attributed to the longer Cr-Sb distance in the HP-I polymorph of 2.834 Å [13]. As the HP-II structure is not stable at 0 GPa, the bulk moduli are also compared at 12 GPa, where the bulk modulus for the HP-II phase is 136(3) GPa and for the HP-I phase 145(1) GPa. Here, the Cr-Sb bond length is still shorter for the HP-II phase, and the slightly higher

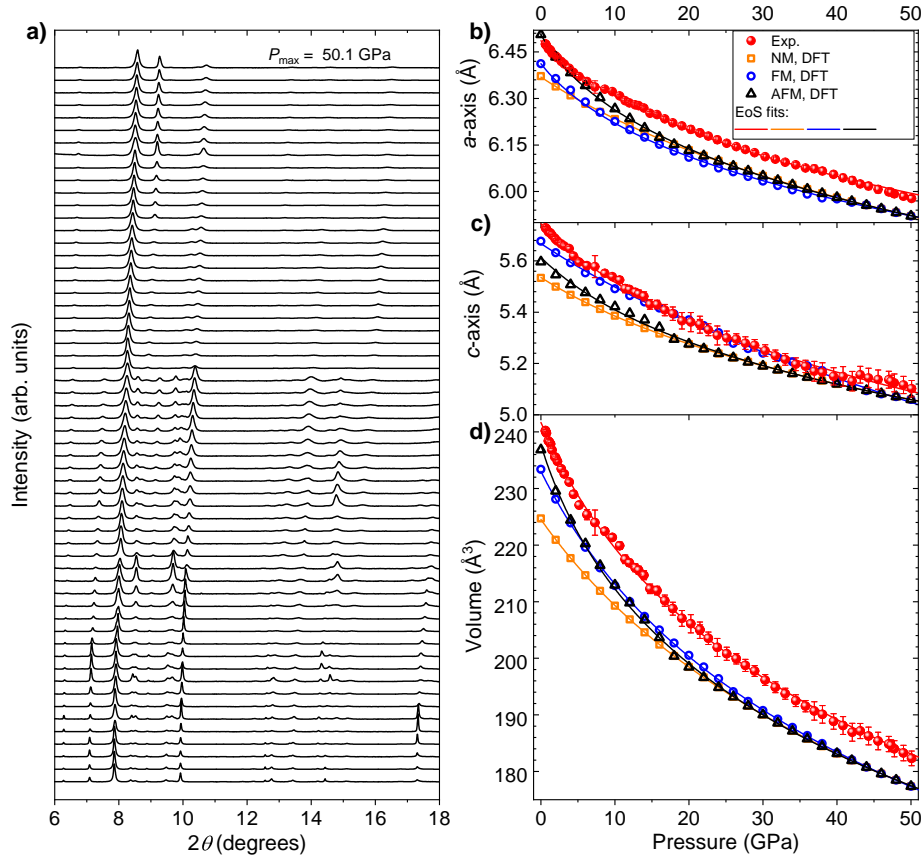


Figure 6: a) Background subtracted waterfall plot of the diffractograms for the HP-I phase. b-d) Experimental and calculated unit cell parameters for the HP-I structure

bulk modulus for the HP-I phase can be explained by its shorter Cr-Cr bond distance.

4. Conclusion

Using single crystal X-ray diffraction at 12 GPa it was shown that the high pressure phase of CrSb_2 crystallizes in the orthorhombic $Cmc2_1$ space group, with a MoP_2 -type structure with unit cell constants of $a = 3.0752(2)$ \AA , $b = 12.4476(19)$ \AA and $c = 5.8741(2)$ \AA well in accordance with the obtained unit cell from DFT calculations and Le Bail refinements of powder diffractograms. Furthermore, electrical resistance measurements under pressure had shown that the phase transition is accompanied by a metallization of the system, and the experimentally measured resistance was verified by resistivity calculations. Furthermore, the calculations showed that the Hall coefficient changes from

Table 4: Bond distances of the different polymorphs of CrSb₂

	Cr-Cr (Å)	Cr-Sb (Å)	Sb-Sb (Å)	Reference
<u>0 GPa</u>				
Marcasite-type	3.2715(7)	2.689(9) ($\times 4$) 2.746(8) ($\times 2$)	2.84(2)	[53]
HP-I (CuAl ₂ -type)	2.8720(2)	2.8339(14)	2.914(9)	[13]
HP-II (MoP ₂ -type) ^a	3.172(13)	2.714(11) 2.729(7) ($\times 2$) 2.772(9) ($\times 2$) 2.743(6) ($\times 2$)	2.907(7)	This study
<u>12 GPa</u>				
HP-I (CuAl ₂ -type)	2.7413(17)	2.7298(7)	2.8431(7)	This study
	3.0751(2)	2.624(7) 2.645(4) ($\times 2$) 2.635(4) ($\times 2$) 2.683(6) ($\times 2$)	2.803(3)	This study
HP-II (MoP ₂ -type)				

^a The values at 0 GPa were obtained using the L_0 values from table S3 and atomic coordinates obtained through SC-XRD.

positive to negative during the phase transition from the marcasite to the MoP₂-type phase.

The calculated band-structure at 12 GPa has shown that this polymorph is a robust type-I Weyl semimetal. Furthermore, the compressibility of both high pressure polymorphs of CrSb₂ were investigated, showing no further phase transitions for both polymorphs, and Le Bail refinements of the unit cell parameters showed that the MoP₂ phase was less compressible than the CuAl₂-type phase which was attributed to the longer Cr-Sb distance in the CuAl₂-type polymorph.

5. Acknowledgements

This research was funded by the Independent Research Fund Denmark (7027-00077B and 1026-00409B) and we furthermore acknowledge the Danish Agency for Science, Technology, and Innovation for funding the instrument center Dan-Scatt. We acknowledge MAX IV Laboratory for beamtime on the DanMAX beamline (Proposal 20211063). Research conducted at MAX IV, a Swedish national user facility, is supported by the Swedish Research council under contract 2018-07152, the Swedish Governmental Agency for Innovation Systems under contract 2018-04969, and Formas under contract 2019-02496. DanMAX is funded by the NUFU grant no. 4059-00009B. Portions of this work were performed at GeoSoilEnviroCARS (The University of Chicago, Sector 13), Advanced Photon Source (APS), Argonne National Laboratory. GeoSoilEnviroCARS is supported

by the National Science Foundation – Earth Sciences (EAR – 1634415). This research used resources of the Advanced Photon Source, a U.S. Department of Energy (DOE) Office of Science User Facility operated for the DOE Office of Science by Argonne National Laboratory under Contract No. DE-AC02-06CH11357. Use of the COMPRES-GSECARS gas loading system was supported by COMPRES under NSF Cooperative Agreement EAR -1606856 and by GSECARS through NSF grant EAR-1634415 and DOE grant DE-FG02-94ER14466. This research used resources of the Advanced Photon Source, a U.S. Department of Energy (DOE) Office of Science User Facility operated for the DOE Office of Science by Argonne National Laboratory under Contract No. DE-AC02-06CH11357. We acknowledge DESY (Hamburg, Germany), a member of the Helmholtz Association HGF, for the provision of experimental facilities. Parts of this research were carried out at PETRA III using the P02.2 beamline. Beamtime was allocated for proposal H-20010016. DC acknowledges support from ICSC – Centro Nazionale di Ricerca in High Performance Computing, Big Data and Quantum Computing, funded by European Union – NextGenerationEU (Grant number CN00000013).

References

- [1] F. Hulliger, New representatives of the NbAs₂ and ZrAs₂ structures, *Nature* 204 (Nov 1964). doi:10.1038/204775a0.
- [2] S. Rundqvist, T. Lundström, X-ray studies of molybdenum and tungsten phosphides, *Acta Chemica Scandinavica* 17 (1963) 37–46. doi:10.3891/acta.chem.scand.17-0037.
- [3] G. Autès, D. Gresch, M. Troyer, A. A. Soluyanov, O. V. Yazyev, Robust type-II weyl semimetal phase in transition metal diphosphides XP₂ (X = Mo, W), *Physical Review Letters* 117 (2016) 066402. doi:10.1103/PhysRevLett.117.066402.
- [4] J. Du, Z. Lou, S. Zhang, Y. Zhou, B. Xu, Q. Chen, Y. Tang, S. Chen, H. Chen, Q. Zhu, H. Wang, J. Yang, Q. Wu, O. V. Yazyev, M. Fang, Extremely large magnetoresistance in the topologically trivial semimetal α -WP₂, *Physical Review B* 97 (2018) 245101. doi:10.1103/PhysRevB.97.245101.
- [5] C. Li, K. Liu, S. Peng, Q. Feng, D. Jiang, T. Wen, H. Xiao, B. Yue, Y. Wang, Rewritable pressure-driven n–p conduction switching in marcasite-type CrSb₂, *Chemistry of Materials* 35 (3) (2023) 1449–1457. doi:10.1021/acs.chemmater.2c03673.
- [6] E. Ehrenreich-Petersen, M. F. Hansen, J. Jeanneau, D. Ceresoli, F. Menescardi, M. Ottesen, V. Prakapenka, S. N. Tkachev, M. Bremholm, Seven-coordinated high-pressure phase of CrSb₂ and experimental equation of state of MSb₂ (M = Cr, Fe, Ru, Os), *Inorganic Chemistry* 62 (31) (2023) 12203–12212. doi:10.1021/acs.inorgchem.3c00227.

- [7] H. Holseth, A. Kjekshus, A. F. Andresen, Compounds with the marcasite type crystal structure. vi. neutron diffraction studies of CrSb_2 and FeSb_2 , *Acta Chemica Scandinavica* 24 (1970) 3309–3316. doi:10.3891/acta.chem.scand.24-3309.
- [8] B. C. Sales, A. F. May, M. A. McGuire, M. B. Stone, D. J. Singh, D. Mandrus, Transport, thermal, and magnetic properties of the narrow-gap semiconductor CrSb_2 , *Physical Review B* 86 (2012) 235136. doi:10.1103/PhysRevB.86.235136.
- [9] K. Nakagawa, M. Kimata, T. Yokouchi, Y. Shiomi, Surface anisotropic magnetoresistance in the antiferromagnetic semiconductor CrSb_2 , *Phys. Rev. B* 107 (2023) L180405. doi:10.1103/PhysRevB.107.L180405. URL <https://link.aps.org/doi/10.1103/PhysRevB.107.L180405>
- [10] H. Takizawa, K. Uheda, T. Endo, M. Shimada, High pressure phase transition of CrSb_2 , *Review of High Pressure Science and Technology/Koatsuryoku No Kagaku To Gijutsu* 7 (1998) 1043–1045. doi:10.4131/jshpreview.7.1043.
- [11] M. Armbrüster, W. Schnelle, U. Schwarz, Y. Grin, Chemical bonding in TiSb_2 and VSb_2 : A quantum chemical and experimental study, *Inorganic Chemistry* 46 (16) (2007) 6319–6328. doi:10.1021/ic070284p.
- [12] W. Xia, X. Shi, Y. Wang, W. Ge, H. Su, Q. Wang, X. Wang, N. Yu, Z. Zou, Y. Hao, W. Zhao, Y. Guo, The de Haas-van Alphen quantum oscillations in a three-dimensional Dirac semimetal TiSb_2 , *Applied Physics Letters* 116 (14) (2020) 142103. doi:10.1063/5.0001566. URL <https://doi.org/10.1063/5.0001566>
- [13] H. Takizawa, K. Uheda, T. Endo, A new ferromagnetic polymorph of CrSb_2 synthesized under high pressure, *Journal of Alloys and Compounds* 287 (1) (1999) 145–149. doi:[https://doi.org/10.1016/S0925-8388\(99\)00056-0](https://doi.org/10.1016/S0925-8388(99)00056-0).
- [14] Y. Y. Jiao, Z. Y. Liu, M. A. McGuire, S. Calder, J.-Q. Yan, B. C. Sales, J. P. Sun, Q. Cui, N. N. Wang, Y. Sui, Y. Uwatoko, B. S. Wang, X. L. Dong, J.-G. Cheng, High-pressure phase of CrSb_2 : A new quasi-one-dimensional itinerant magnet with competing interactions, *Physical Review Materials* 3 (2019) 074404. doi:10.1103/PhysRevMaterials.3.074404.
- [15] N. Kumar, Y. Sun, N. Xu, K. Manna, M. Yao, V. Süß, I. Leermakers, O. Young, T. Förster, M. Schmidt, H. Borrmann, B. Yan, U. Zeitler, M. Shi, C. Felser, C. Shekhar, Extremely high magnetoresistance and conductivity in the type-II weyl semimetals WP_2 and MoP_2 , *Nature Communications* 8 (Nov 2017). doi:10.1038/s41467-017-01758-z.
- [16] Y.-Y. Lv, J. Xu, S. Han, C. Zhang, Y. Han, J. Zhou, S.-H. Yao, X.-P. Liu, M.-H. Lu, H. Weng, Z. Xie, Y. B. Chen, J. Hu, Y.-F. Chen,

- S. Zhu, High-harmonic generation in weyl semimetal β -WP₂ crystals, Nature Communications 12 (2021) 6437. doi:<https://doi.org/10.1038/s41467-021-26766-y>.
- [17] A. Toniato, B. Gotsmann, E. Lind, C. B. Zota, Weyl semi-metal-based high-frequency amplifiers, in: 2019 IEEE International Electron Devices Meeting (IEDM), 2019, pp. 9.4.1–9.4.4. doi:[10.1109/IEDM19573.2019.8993575](https://doi.org/10.1109/IEDM19573.2019.8993575).
- [18] X. Liu, Z. Yu, J. Li, Z. Xu, C. Zhou, Z. Dong, L. Zhang, X. Wang, N. Yu, Z. Zou, X. Wang, Y. Guo, A new transition metal diphosphide α -MoP₂ synthesized by a high-temperature and high-pressure technique, Chinese Physics B 32 (1) (2023) 018102. doi:[10.1088/1674-1056/ac633d](https://doi.org/10.1088/1674-1056/ac633d). URL <https://dx.doi.org/10.1088/1674-1056/ac633d>
- [19] Z. Chi, J. Zhang, Z. Gong, F. Peng, X. Wang, G. Dong, Y. Li, Y. Shi, Y. Ge, X. Yang, Z. Zhang, G. Xu, N. Hao, C. Zhou, J. Qin, Pressure-induced Lifshitz transition in the type-II Weyl semimetal WP₂, Materials Today Physics 42 (2024) 101372. doi:<https://doi.org/10.1016/j.mtphys.2024.101372>. URL <https://www.sciencedirect.com/science/article/pii/S2542529324000488>
- [20] K. D. Leinenweber, J. A. Tyburczy, T. G. Sharp, E. Soignard, T. Diedrich, W. B. Petuskey, Y. Wang, J. L. Mosenfelder, Cell assemblies for reproducible multi-anvil experiments (the COMPRES assemblies), American Mineralogist 97 (2-3) (2012) 353–368. doi:[10.2138/am.2012.3844](https://doi.org/10.2138/am.2012.3844).
- [21] H.-P. Liermann, Z. Konôpková, W. Morgenroth, K. Glazyrin, J. Bednarčík, E. E. McBride, S. Petitgirard, J. T. Delitz, M. Wendt, Y. Bican, A. Ehnes, I. Schwark, A. Rothkirch, M. Tischer, J. Heuer, H. Schulte-Schrepping, T. Kracht, H. Franz, The Extreme Conditions Beamline P02.2 and the Extreme Conditions Science Infrastructure at PETRAIII, Journal of Synchrotron Radiation 22 (4) (2015) 908–924. doi:[10.1107/S1600577515005937](https://doi.org/10.1107/S1600577515005937).
- [22] K. Syassen, Ruby under pressure, High Pressure Research 28 (2) (2008) 75–126. doi:[10.1080/08957950802235640](https://doi.org/10.1080/08957950802235640).
- [23] CrysAlisPRO, Oxford Diffraction /Agilent Technologies UK Ltd, Yarnton, England.
- [24] O. V. Dolomanov, L. J. Bourhis, R. J. Gildea, J. A. K. Howard, H. Puschmann, *OLEX2*: a complete structure solution, refinement and analysis program, Journal of Applied Crystallography 42 (2) (2009) 339–341. doi:[10.1107/S0021889808042726](https://doi.org/10.1107/S0021889808042726).
- [25] G. M. Sheldrick, Crystal structure refinement with *SHELXL*, Acta Crystallographica Section C 71 (1) (2015) 3–8. doi:[10.1107/S2053229614024218](https://doi.org/10.1107/S2053229614024218).

- [26] G. M. Sheldrick, *SHELXT* – Integrated space-group and crystal-structure determination, *Acta Crystallographica Section A* 71 (1) (2015) 3–8. doi:10.1107/S2053273314026370.
- [27] M. Rivers, V. B. Prakapenka, A. Kubo, C. Pullins, C. M. Holl, S. D. Jacobsen, The COMPRES/GSECARS gas-loading system for diamond anvil cells at the advanced photon source, *High Pressure Research* 28 (3) (2008) 273–292. doi:10.1080/08957950802333593.
- [28] A. Dewaele, P. Loubeyre, M. Mezouar, Equations of state of six metals above 94 GPa, *Physical Review B* 70 (2004) 094112. doi:10.1103/PhysRevB.70.094112.
- [29] Y. Fei, A. Ricolleau, M. Frank, K. Mibe, G. Shen, V. Prakapenka, Toward an internally consistent pressure scale, *Proceedings of the National Academy of Sciences* 104 (22) (2007) 9182–9186. doi:10.1073/pnas.0609013104.
- [30] C. Prescher, V. B. Prakapenka, DIOPTAS: a program for reduction of two-dimensional x-ray diffraction data and data exploration, *High Pressure Research* 35 (3) (2015) 223–230. doi:10.1080/08957959.2015.1059835.
- [31] J. Rodríguez-Carvajal, Recent advances in magnetic structure determination by neutron powder diffraction, *Physica B: Condensed Matter* 192 (1) (1993) 55–69. doi:https://doi.org/10.1016/0921-4526(93)90108-I.
- [32] J. Gonzalez-Platas, M. Alvaro, F. Nestola, R. Angel, *EosFit7-GUI*: a new graphical user interface for equation of state calculations, analyses and teaching, *Journal of Applied Crystallography* 49 (4) (2016) 1377–1382. doi:10.1107/S1600576716008050.
- [33] K. Momma, F. Izumi, *VESTA3* for three-dimensional visualization of crystal, volumetric and morphology data, *Journal of Applied Crystallography* 44 (6) (2011) 1272–1276. doi:10.1107/S0021889811038970.
- [34] S. T. Weir, J. Akella, C. Aracne-Ruddle, Y. K. Vohra, S. A. Catledge, Epitaxial diamond encapsulation of metal microprobes for high pressure experiments, *Applied Physics Letters* 77 (21) (2000) 3400–3402. doi:10.1063/1.1326838.
- [35] P. Giannozzi, S. Baroni, N. Bonini, M. Calandra, R. Car, C. Cavazzoni, D. Ceresoli, G. L. Chiarotti, M. Cococcioni, I. Dabo, A. D. Corso, S. de Gironcoli, S. Fabris, G. Fratesi, R. Gebauer, U. Gerstmann, C. Gougoussis, A. Kokalj, M. Lazzeri, L. Martin-Samos, N. Marzari, F. Mauri, R. Mazzarello, S. Paolini, A. Pasquarello, L. Paulatto, C. Sbraccia, S. Scandolo, G. Sclauzero, A. P. Seitsonen, A. Smogunov, P. Umari, R. M. Wentzcovitch, QUANTUM ESPRESSO: a modular and open-source software project for quantum simulations of materials, *Journal of Physics: Condensed Matter* 21 (39) (2009) 395502. doi:10.1088/0953-8984/21/39/395502.

- [36] P. Giannozzi, O. Andreussi, T. Brumme, O. Bunau, M. B. Nardelli, M. Calandra, R. Car, C. Cavazzoni, D. Ceresoli, M. Cococcioni, N. Colonna, I. Carnimeo, A. D. Corso, S. de Gironcoli, P. Delugas, R. A. DiStasio, A. Ferretti, A. Floris, G. Fratesi, G. Fugallo, R. Gebauer, U. Gerstmann, F. Giustino, T. Gorni, J. Jia, M. Kawamura, H.-Y. Ko, A. Kokalj, E. Küçükbenli, M. Lazzeri, M. Marsili, N. Marzari, F. Mauri, N. L. Nguyen, H.-V. Nguyen, A. O. de-la Roza, L. Paulatto, S. Poncé, D. Rocca, R. Sabatini, B. Santra, M. Schlipf, A. P. Seitsonen, A. Smogunov, I. Timrov, T. Thonhauser, P. Umari, N. Vast, X. Wu, S. Baroni, Advanced capabilities for materials modelling with QUANTUM ESPRESSO, *Journal of Physics: Condensed Matter* 29 (46) (2017) 465901. doi:10.1088/1361-648x/aa8f79.
- [37] J. P. Perdew, A. Ruzsinszky, G. I. Csonka, O. A. Vydrov, G. E. Scuseria, L. A. Constantin, X. Zhou, K. Burke, Restoring the density-gradient expansion for exchange in solids and surfaces, *Physical Review Letters* 100 (2008) 136406. doi:10.1103/PhysRevLett.100.136406.
- [38] G. Kuhn, S. Mankovsky, H. Ebert, M. Regus, W. Bensch, Electronic structure and magnetic properties of CrSb₂ and FeSb₂ investigated via ab initio calculations, *Physical Review B* 87 (8) (feb 2013). doi:10.1103/physrevb.87.085113.
- [39] G. K. Madsen, J. Carrete, M. J. Verstraete, BoltzTraP2, a program for interpolating band structures and calculating semi-classical transport coefficients, *Computer Physics Communications* 231 (2018) 140–145. doi:10.1016/j.cpc.2018.05.010.
- [40] F. T. Cerasoli, A. R. Supka, A. Jayaraj, M. Costa, I. Siloi, J. Sławińska, S. Curtarolo, M. Fornari, D. Ceresoli, M. B. Nardelli, Advanced modeling of materials with PAOFLOW 2.0: New features and software design, *Computational Materials Science* 200 (2021) 110828. doi:10.1016/j.commatsci.2021.110828.
- [41] D. Gresch, G. Autès, O. V. Yazyev, M. Troyer, D. Vanderbilt, B. A. Bernevig, A. A. Soluyanov, Z2pack: Numerical implementation of hybrid wannier centers for identifying topological materials, *Physical Review B* 95 (7) (feb 2017). doi:10.1103/physrevb.95.075146.
- [42] H. R. Aliabad, S. Rabbanifar, M. Khalid, Structural, optoelectronic and thermoelectric properties of FeSb₂ under pressure: Bulk and monolayer, *Physica B: Condensed Matter* 570 (2019) 100–109. doi:https://doi.org/10.1016/j.physb.2019.06.001.
- [43] A. Mani, J. Janaki, A. T. Satya, T. G. Kumary, A. Bharathi, The pressure induced insulator to metal transition in FeSb₂, *Journal of Physics: Condensed Matter* 24 (7) (2012) 075601. doi:10.1088/0953-8984/24/7/075601.
- [44] L.-D. Yuan, Z. Wang, J.-W. Luo, A. Zunger, Prediction of low-Z collinear and noncollinear antiferromagnetic compounds having momentum-dependent

- spin splitting even without spin-orbit coupling, *Physical Review Materials* 5 (1) (jan 2021). doi:10.1103/physrevmaterials.5.014409.
- [45] I. I. Mazin, K. Koepf, M. D. Johannes, R. González-Hernández, L. Šmejkal, Prediction of unconventional magnetism in doped FeSb₂, *Proceedings of the National Academy of Sciences* 118 (42) (oct 2021). doi:10.1073/pnas.2108924118.
- [46] V. Soto, K. Knorr, L. Ehm, C. Baehtz, B. Winkler, M. Avalos-Borja, High-pressure and high-temperature powder diffraction on molybdenum diphosphide, MoP₂, *Zeitschrift für Kristallographie - Crystalline Materials* 219 (6) (2004) 309–313. doi:doi:10.1524/zkri.219.6.309.34642.
- [47] A. Tavassoli, A. Grytsiv, F. Failamani, G. Rogl, S. Puchegger, H. Müller, P. Broz, F. Zelenka, D. Macciò, A. Saccone, G. Giester, E. Bauer, M. Zehetbauer, P. Rogl, Constitution of the binary m-sb systems (m = Ti, Zr, Hf) and physical properties of MSb₂, *Intermetallics* 94 (2018) 119–132. doi:https://doi.org/10.1016/j.intermet.2017.12.014.
- [48] F. Failamani, P. Broz, D. Macciò, S. Puchegger, H. Müller, L. Salamakha, H. Michor, A. Grytsiv, A. Saccone, E. Bauer, G. Giester, P. Rogl, Constitution of the systems {V,Nb,Ta}-Sb and physical properties of diantimonides {V,Nb,Ta}Sb₂, *Intermetallics* 65 (2015) 94–110. doi:https://doi.org/10.1016/j.intermet.2015.05.006.
- [49] Y. Grin, F. R. Wagner, M. Armbrüster, M. Kohout, A. Leithe-Jasper, U. Schwarz, U. Wedig, H. Georg von Schnering, CuAl₂ revisited: Composition, crystal structure, chemical bonding, compressibility and raman spectroscopy, *Journal of Solid State Chemistry* 179 (6) (2006) 1707–1719. doi:https://doi.org/10.1016/j.jssc.2006.03.006.
- [50] Y. K. Vohra, P. T. Spencer, Novel γ -phase of titanium metal at megabar pressures, *Physical Review Letters* 86 (2001) 3068–3071. doi:10.1103/PhysRevLett.86.3068.
- [51] W. A. Crichton, J. Guignard, E. Bailey, D. P. Dobson, S. A. Hunt, A. R. Thomson, High-temperature equation of state of vanadium, *High Pressure Research* 36 (1) (2016) 16–22. doi:10.1080/08957959.2015.1123256.
- [52] A. Marizy, G. Geneste, P. Loubeyre, B. Guigue, G. Garbarino, Synthesis of bulk chromium hydrides under pressure of up to 120 GPa, *Physical Review B* 97 (2018) 184103. doi:10.1103/PhysRevB.97.184103.
- [53] H. Holseth, A. Kjekshus, Compounds with the marcasite type crystal structure. II. on the crystal structures of the binary pnictides, *Acta Chemica Scandinavica* 22 (1968) 3284–3292. doi:10.3891/acta.chem.scand.22-3284.